

**\*\*TITLE\*\***  
*ASP Conference Series, Vol. \*\*VOLUME\*\*, \*\*PUBLICATION YEAR\*\**  
**\*\*EDITORS\*\***

## Chandra X-ray Observations of Cygnus A and Pictor A

A. S. Wilson

*Astronomy Department, University of Maryland, College Park, MD  
20742, U.S.A. and Space Telescope Science Institute, 3700 San Martin  
Drive, Baltimore, MD 21218, U.S.A.*

A. J. Young

*Astronomy Department, University of Maryland, College Park, MD  
20742, U.S.A.*

P. L. Shopbell

*Department of Astronomy, California Institute of Technology, MS  
105-24, Pasadena, CA 91125*

**Abstract.** Results from Chandra observations of the two nearest, powerful radio galaxies are summarised.

### 1. Introduction

The talk described observations of Cygnus A ( $z = 0.0562$ ) and Pictor A ( $z = 0.035$ ) with the Chandra X-ray Observatory. Since the early results from these observations are published (Wilson, Young & Shopbell 2000, 2001), we here confine ourselves to a summary of the main conclusions and a few remarks about other aspects of the results on Cygnus A, which will be amplified in a future paper.

### 2. Cygnus A

#### 2.1. Cavity, Hot Spots, Jets and Nucleus

The Chandra image of Cygnus A is shown in Fig. 1. This figure shows only the region of the radio source and omits the large-scale, X-ray emitting gas which comprises the intracluster medium. The dominant feature of Fig. 1 is a limb-brightened, elliptical (presumably prolate-spheroidal in three dimensions) structure. The major axis coincides with that of the radio source and the radio hot spots are seen as compact X-ray sources at the ends of the major axis. This structure appears to be the observational manifestation of the cavity which is expected to be inflated in the intracluster medium by relativistic material which has passed through the hot spots at the ends of the jets. Its existence and dynamics were first inferred and explored in the classic paper by Scheuer (1974). The ratio of major to minor axis of the ellipse is  $\sim 2 - 2.5$ , in agreement with the expectations of simple models (cf. Begelman & Cioffi 1989). Bright, curved

bands of emission project along the minor axis of the ellipse. It is tempting to interpret these features as “belts” of gas extending around the equator of the prolate spheroidal structure.

A curved structure runs along the major axis from the nucleus to each pair of hot spots. These two features are apparently the X-ray manifestations of the jets. They are, however, broad, diffuse and of low contrast, quite unlike the sharply defined radio structure of the large scale NW (the near side of the radio source) jet (cf. Carilli et al. 1996). The X-ray jet almost disappears near the NW hot spots (A and B in the nomenclature of Hargrave & Ryle 1974). There is also a faint elliptical semi-ring in the X-ray image; this semi-ring extends  $\simeq 10''$  to the NE of hot spots A and B. The combination of this structure and the two hot spots resembles a set of ‘headphones’ (the hot spots mark the ‘earpieces’). Definitive statements cannot be made in view of the low contrast of the X-ray jets, but we speculate that either:

a) the NW jet is continuous and steady but much broader than would be inferred from the radio maps. In this interpretation, the hot spots and the semi-ring reflect the interaction of the outer annulus of the jet with the intracluster gas. The observed radio jets and hot spots might then be effects of limb-brightening at the edges of the broad jet (cf. Blandford [1996] who suggests that the hot spots might be a ring vortex seen in projection). However, the great brightness of the hot spots and the close agreement between their radio synchrotron and X-ray synchrotron self-Compton emissions (see next subsection) challenge a limb-brightening interpretation. Alternatively, an absence of radio emission from the center of the jet may mean that the jet is actually hollow or that the jet’s center comprises material uncondusive to radio emission.

or: b) the NW jet is intrinsically narrow, as inferred from the radio maps, but the direction in which it is launched is continuously changing (precession of the nozzle?), so that its terminus traces out a circle where it meets the intracluster gas. The elliptical semi-ring is then the projection of this terminal circle, and the hot spots are two locations along the circle where the radio emission is unusually bright, as a result of projection or other effects.

The X-ray nucleus is extended in the SE - NW direction. Its spectrum is shown in Fig. 2. The high energy continuum may be modeled as an absorbed power law, as known from previous work (e.g. Arnaud 1996). Notable features include: a) a  $K\alpha$  line from neutral or lowly ionized iron (seen in the observed spectrum near 6.0 keV), b) strong K edge absorption from neutral or lowly ionized iron (observed near 7.0 keV), and c) emission at energies below 2 keV in excess of that expected from the absorbed power law. Emission lines, which are confirmed in an independent spectrum with higher signal to noise at low energies, are apparent and tentatively identified with  $K\alpha$  transitions of silicon, neon and possibly magnesium. The soft X-ray emission apparently originates from an extended region viewed through a relatively low absorbing column.

## 2.2. Synchrotron Self-Compton Emission from the Hot Spots

Fig. 3 (left) shows X-ray contours on a grey scale of a 6 cm image with resolution  $0''.35$  (Perley, Dreher & Cowan 1984) in the vicinities of the western hot spots (A and B). The extents and morphologies of the X-ray and radio hot spots are very similar, with the directions of elongation agreeing to within a few degrees.

Similar results are obtained for hot spots D and E. The X-ray spectra of hot spots A and D have been modeled with an absorbed power law. In both cases, the absorbing column is  $N_{\text{H}} = 3.3 \times 10^{21} \text{ cm}^{-2}$ , in excellent agreement with the Galactic column in the direction of Cygnus A. The photon indices are also similar at  $\Gamma = 1.8 \pm 0.2$ .

Thermal models for the X-ray emission may be ruled out as they require too high gas densities. Fig. 3 (right) shows the results of calculation of a synchrotron self-Compton (SSC) model for hot spot A. As may be seen, the predicted SSC radiation is in excellent agreement with the Chandra-observed spectrum for a magnetic field of  $1.5 \times 10^{-4}$  gauss. This value may be compared with the equipartition value of  $2.8 \times 10^{-4}$  gauss in hot spot A, calculated assuming no relativistic protons, the broken power-law spectra of Carilli et al. (1991), low frequency cut-offs at 10 MHz and high frequency cut-offs at 400 GHz. The uncertainty in the magnetic field strength estimated from the SSC model is estimated to be a few tens of percent.

The most straightforward interpretation is that the relativistic gas is an electron-positron plasma and is close to equipartition with the magnetic field. If, on the other hand, the energy in relativistic protons dominates that in relativistic electrons and the X-rays are still SSC radiation, the energy density in relativistic protons must exceed that in the magnetic field. It is notable that the magnetic field cannot be less than  $1.5 \times 10^{-4}$  gauss since the SSC radiation would then exceed the observed X-radiation.

The alternative is that  $B > 1.5 \times 10^{-4}$  gauss in which case the predicted SSC emission would be too weak to account for the observed X-ray emission. The X-rays would then have to be synchrotron radiation. However, in view of the excellent agreement between the SSC model and the observations, we consider a synchrotron model implausible.

### 3. Pictor A

Fig. 4 shows the Chandra image of the nucleus, western jet and western hot spot of Pictor A (much fainter X-ray emission is found to the east of the nucleus - see Wilson, Young & Shopbell 2001). The jet extends at least  $1'.9$  (110 kpc) westward from the nucleus and is spatially coincident with the faint radio jet (Perley, Röser & Meisenheimer 1997). The X-ray jet “points” at the western hot spot, which is  $4'.2$  (240 kpc) from the nucleus. When the nuclear X-ray source is shifted slightly to coincide with the nuclear radio source, the peak of the X-ray emission from the hot spot is within  $1''$  of its radio peak.

Images of the western hot spot at radio, optical (Röser 1989; Perley, Röser & Meisenheimer 1997) and X-ray wavelengths with similar resolutions are shown in Fig. 5. As may be seen, the overall X-ray morphology is remarkably similar to the radio and optical. The high linear polarization of the hot spot at both radio and optical wavelengths indicates that the emission is synchrotron radiation in these wavebands.

Fig. 6 shows the broad band spectrum of the western hot spot. The radio spectrum of the hot spot is well described by a power law with  $\alpha = 0.740 \pm 0.015$  (Meisenheimer, Yates & Röser 1997), but there must be a break or turnover in the spectrum at  $10^{13-14}$  Hz to accommodate the near infrared and

optical measurements. It is also apparent that the X-ray spectrum is not a simple extension of the radio and optical measurements to higher frequencies.

Wilson, Young & Shopbell (2001) reached the following conclusions about the X-ray emission of the hot spot, assuming that its bulk outward motion is non-relativistic. (i) Inverse Compton scattering of the synchrotron radio photons by the relativistic electrons responsible for the radio emission (i.e. a synchrotron self-Compton model) may be ruled out for the hot spot's X-ray emission, as the predicted spectrum differs from that observed. (ii) A successful inverse Compton model may be constructed for the X-ray emission by invoking a low energy population of relativistic electrons with an energy index appropriate to the X-ray spectral index. However, the magnetic field must be reduced to  $\sim 1\%$  of equipartition, and there is no evidence for such an electron population. (iii) The emission may be reproduced in a composite synchrotron plus synchrotron self-Compton model (solid line in Fig. 6). However, the model is contrived, requiring similar fluxes from the two components in the Chandra band. (iv) Synchrotron radiation is possible, but the electron population must be distinct from that which produces the radio and optical emission. However, the X-ray spectrum is in excellent agreement with the expected form if the electrons are accelerated by strong shocks. Relativistic electrons may also result from a 'proton induced cascade' (e. g. Mannheim, Krüßls & Biermann 1991).

If the jet is non-relativistic, inverse Compton scattering is an implausible model for its X-ray emission, for it requires a magnetic field a factor of 30 below equipartition. Further, it is hard to understand why the jet is brighter than the lobe (the opposite of the situation in the radio) in such a model. If the jet is relativistic, these difficulties are eased, and we consider inverse Compton scattering by such a jet off the microwave background a viable mechanism. However, the magnetic field must still be well below equipartition for plausible angles between the jet and the line of sight in this lobe-dominated, FR II radio galaxy. Synchrotron radiation is another possibility.

#### 4. The difference between the hot spots of Cygnus A and Pictor A

It is striking that the X-ray emissions from the hot spots of Cygnus A, 3C 123 (Hardcastle, Birkinshaw & Worrall 2000) and 3C 295 (Harris et al. 2000) conform to an SSC model with a magnetic field close to equipartition (calculated assuming that only electrons are present). In three other galaxies - Pictor A, 3C 120 (Harris et al. 1999) and 3C 390.3 (Harris, Leighly & Leahy 1998) - the X-ray emission is orders of magnitude too strong to be SSC emission with an equipartition magnetic field. While this is a small sample, we (Wilson, Young & Shopbell 2000) noted that 3C 295 and Cygnus A are in clusters with prominent cooling flows and 3C 123 is in a cluster with strong, extended X-ray emission and thus may be within a cooling flow. In contrast, Pictor A, 3C 120 and 3C 390.3 are not in cooling flows. Such an environmental difference could affect the X-ray power from the hot spots in two ways: (a) the presence of high density surrounding gas may inhibit production of X-ray synchrotron emitting electrons in hot spots, or (b) the environments of the "overluminous" X-ray hot spots might have such low gas density that the bulk outward motion of the hot spots is relativistic. Luminous X-ray emission could then originate through inverse

Compton scattering of the microwave background radiation, as we have discussed for the *jet* of Pictor A. In the second case, objects with high X-ray to radio flux ratios would tend to be viewed more pole-on than objects with low X-ray to radio flux ratios. Chandra observations of a larger sample of hot spots should cast light on these issues.

This research was supported by NASA grant NAG 81027 and by the Graduate School of the University of Maryland. We are grateful to Rick Perley for providing his radio images.

## References

- Arnaud, K. 1996, 'X-ray evidence for a buried quasar in Cygnus A', in *Cygnus A - Study of a Radio Galaxy*, ed. C. L. Carilli and D. E. Harris (Cambridge University Press), 51–55
- Begelman, M. C. & Cioffi, D. F. 1989, 'Overpressured Cocoons in Extragalactic Radio Sources' *ApJ*, 345, L21–L24
- Blandford, R. D. 1996, 'The Untangling of Cygnus A', in *Cygnus A - Study of a Radio Galaxy*, ed. C. L. Carilli and D. E. Harris (Cambridge University Press), 264–274
- Carilli, C. L., Perley, R. A., Dreher, J. W. & Leahy, J. P. 1991, 'Multifrequency Radio Observations of Cygnus A: Spectral Aging in Powerful Radio Galaxies', *ApJ*, 383, 554–573
- Carilli, C. L., Perley, R. A., Bartel, N. & Dreher, J. W. 1996, 'The Jets in Cygnus A: from pc- to kpc-scales' in *Cygnus A - Study of a Radio Galaxy*, ed. C. L. Carilli and D. E. Harris (Cambridge University Press), 76–85
- Hardcastle, M. J., Birkinshaw, M. & Worrall, D. M. 2000, 'A Chandra detection of the radio hotspot of 3C123', *MNRAS*, submitted (2000)
- Hargrave, P. J. & Ryle, M. 1974, 'Observations of Cygnus A with the 5-km Radio Telescope' *MNRAS*, 166, 305–327
- Harris, D. E., Leighly, K. M. & Leahy, J. P. 1998, 'X-ray Emission from a Radio Hot Spot in 3C390.3: Evidence for the Deflection of a Radio Jet by a Neighboring Galaxy' *ApJ*, 499, L149–L152
- Harris, D. E., Hjorth, J., Sadun, A. C., Silverman, J. D. & Vestergaard, M. 1999, 'X-ray Emission from the Radio Jet in 3C120', *ApJ*, 518, 213–218
- Harris, D. E. et al. 2000, 'Chandra X-ray Detection of the Radio Hot Spots of 3C295', *ApJ*, 530, L81–L84
- Mannheim, K., Krülls, W. M. & Biermann, P. L. 1991, 'A novel mechanism for non-thermal X-ray emission', *A&A*, 251, 723–731
- Meisenheimer, K., Yates, M. G. & Röser, H.-J. 1997, 'The synchrotron spectra of radio hot spots. II. Infrared imaging', *A&A*, 325, 57–73
- Perley, R. A., Dreher, J. W. & Cowan, J. J. 1984, 'The Jet and Filaments in Cygnus A' *ApJ*, 285, L35–L38
- Perley, R. A., Röser, H.-J. & Meisenheimer, K. 1997, 'The Radio Galaxy Pictor A - a Study with the VLA' *A&A*, 328, 12–32

- Röser, H.-J. 1989, ‘Continuum Observations of Hot Spots at Wavelengths  $< 1$  cm’ in *Lecture Notes in Physics* vol. 327, *Hot Spots in Extragalactic Radio Sources*, eds. Meisenheimer, K. & Röser, H.-J. (Springer-Verlag) 91–114
- Scheuer, P. A. G. 1974, ‘Models of Extragalactic Radio Sources with a Continuous Energy Supply from a Central Object’ *MNRAS*, 166, 513–528
- Wilson, A. S., Young, A. J. & Shopbell, P. L. 2000, ‘Chandra Observations of Cygnus A: Magnetic Field Strengths in the Hot Spots of a Radio Galaxy’ *ApJ*, 544, L27–L30
- Wilson, A. S., Young, A. J. & Shopbell, P. L. 2001, ‘Chandra X-ray Observations of Pictor A: High Energy Cosmic Rays in a Radio Galaxy?’ *ApJ*(in press for Feb 1 2001 issue; also available as astro-ph/0008467)

## Figure Captions

Figure 1. A grey scale representation of the Chandra X-ray image of Cygnus A. The shading is proportional to the square root of the intensity. Coordinates are for epoch J2000.0 throughout this paper.

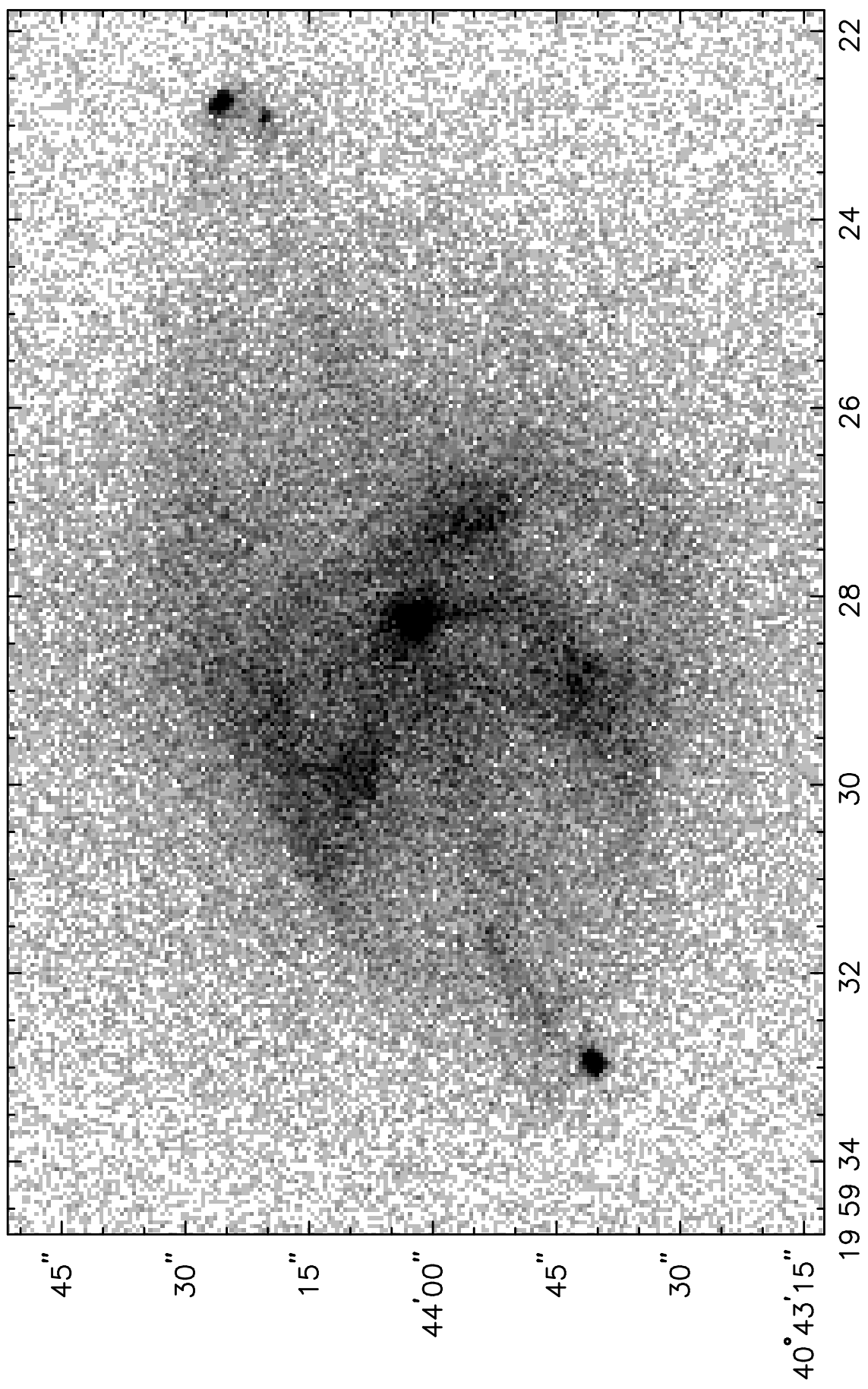
Figure 2. Chandra X-ray spectrum of the nucleus of Cygnus A. The x axis represents observed photon energy. The upper panel shows the data [points with error bars] and a model of an absorbed power law spectrum folded through the instrumental response (solid line). The lower panel shows the deviations of the observed spectrum from the model. Our study of the nuclear spectrum is in collaboration with Keith Arnaud.

Figure 3. *a*: X-ray emission (contours) superposed on a 6 cm VLA radio map (grey scale) of the region of the western hot spots (A, the brighter, and B,  $\simeq 6''$  SE of A) in Cygnus A. Contours are plotted at 2, 4, 8, 12, 16, 24 and 32 counts per pixel ( $0''.5 \times 0''.5$ ). The grey scale is proportional to the square root of the radio brightness. *b*: Spectrum of hot spot A. The points show the radio fluxes and the line through them the model of the synchrotron radiation. The “bow tie” is the Chandra measured boundary of the X-ray spectrum (these error lines are 90% confidence after freezing  $N_{\text{H}}$  at its best fit value, which coincides with the Galactic column). The solid line is the predicted SSC spectrum for  $\gamma_{\text{min}} = 1$  and the dashed line for  $\gamma_{\text{min}} = 100$ .

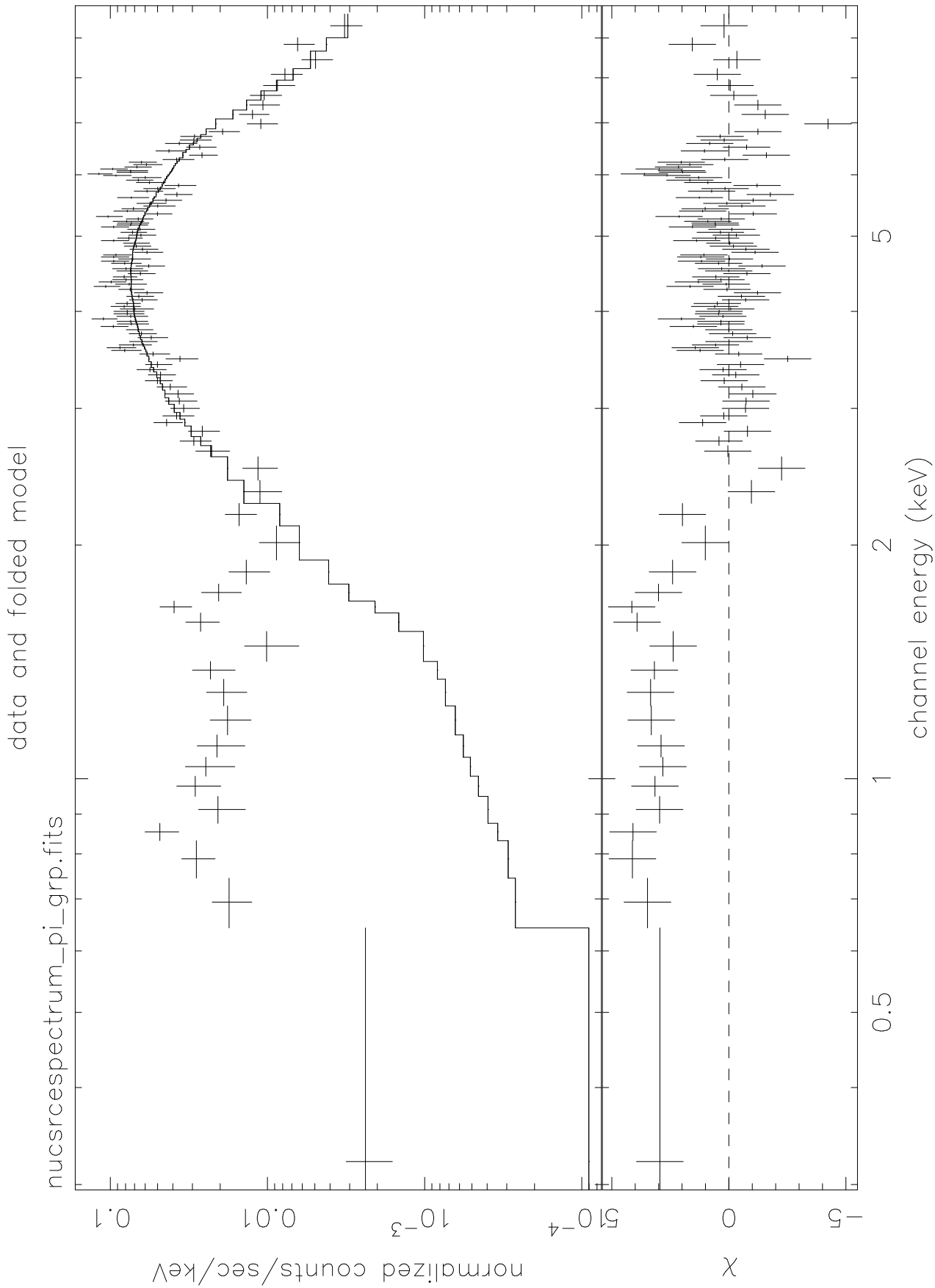
Figure 4. Grey scale representation of the full resolution Chandra image of the nucleus, jet and western hot spot of Pictor A.

Figure 5. The morphology of the western hotspot of Pictor A, at 3.6 cm radio (left panels; PRM), R band optical (center panels; Röser (1989) and PRM) and X-ray (right panels; this paper) wavelengths. The upper panels are grey scale representations and the lower panels are contour plots in which the contours are logarithmically spaced and separated by a factor of 2. The radio and optical images have a FWHM resolution  $\simeq 1''.5$  (shown as the filled circles at the bottom right) and the X-ray image has a FWHM of  $1''.2 \times 1''.9$  (the PSF is shown at the bottom right; no smoothing has been applied to the X-ray image).

Figure 6. The broad band spectrum, plotted as  $\nu S_{\nu}$ , of the western hotspot of Pictor A from radio through X-ray wavelengths. Note that the scale along the y axis is expanded compared to that along the x axis. The circular and triangular symbols are measured data points, while the “bow tie” represents the Chandra spectrum. The lines represent various models discussed in Wilson, Young & Shopbell (2001).

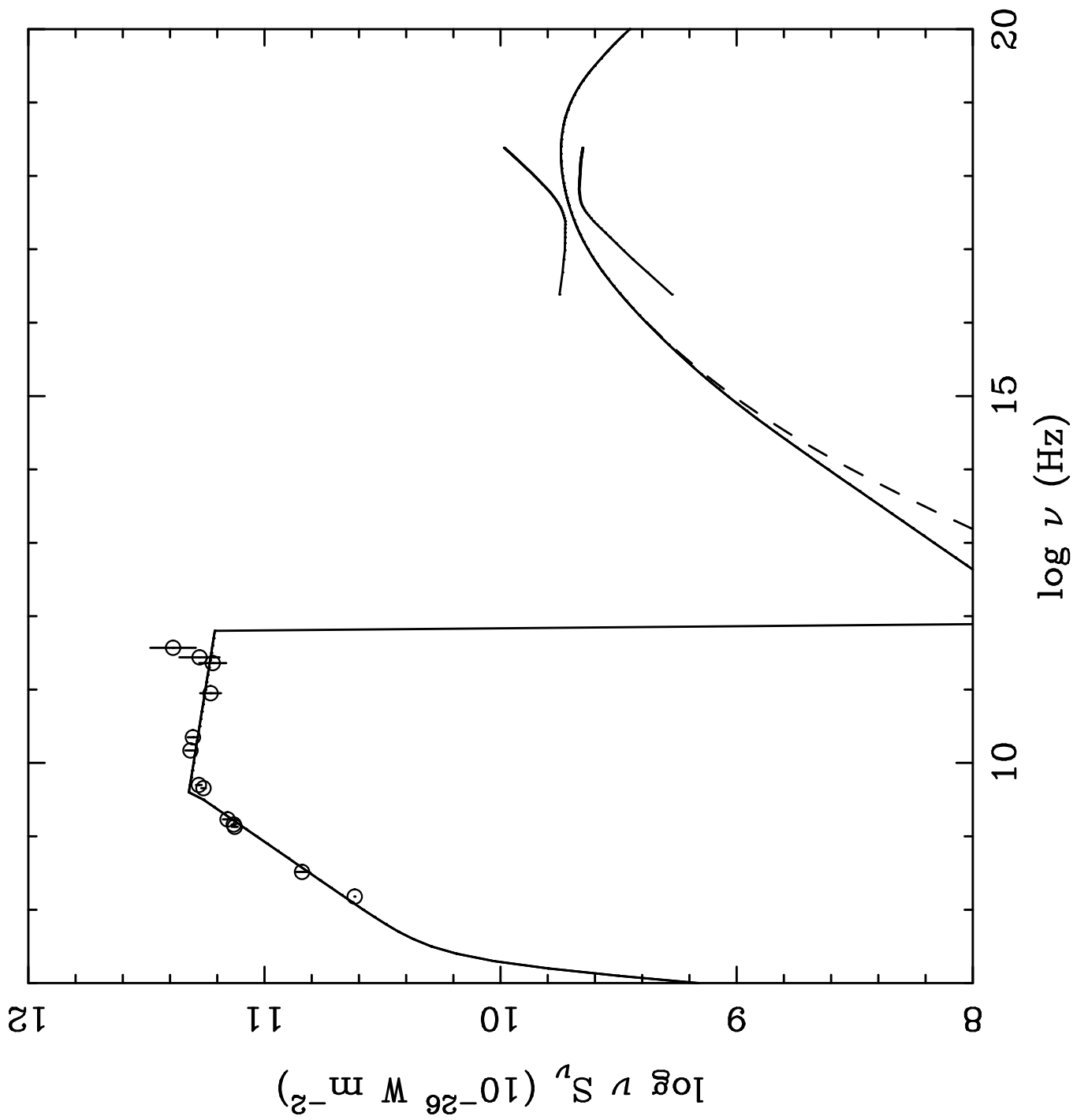


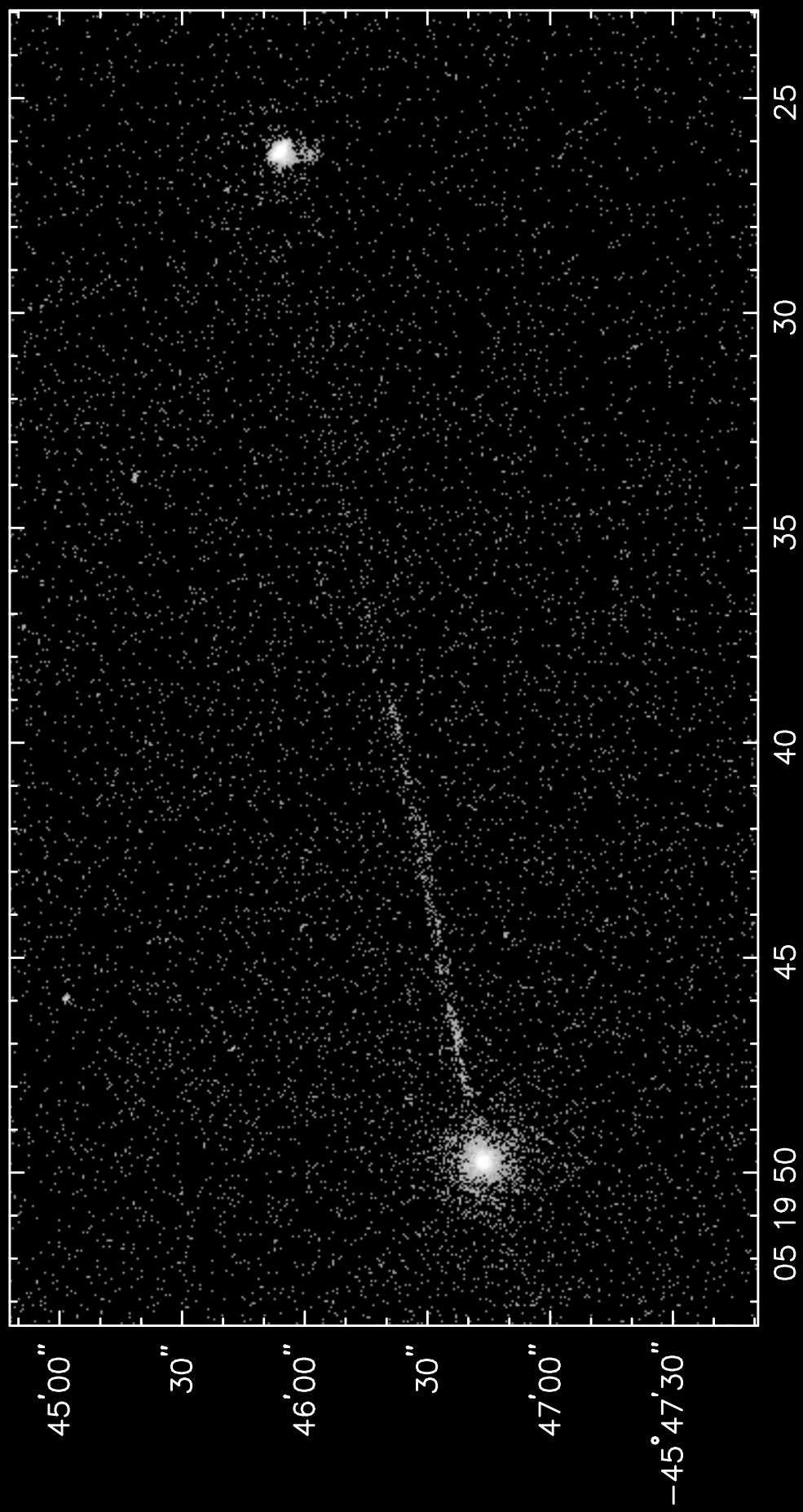




This figure "figure3a.gif" is available in "gif" format from:

<http://arxiv.org/ps/astro-ph/0101422v1>





This figure "figure5.gif" is available in "gif" format from:

<http://arxiv.org/ps/astro-ph/0101422v1>

